ADVANCED FUNCTIONAL MATERIALS
www.afm-journal.de

3D Printing of Ordered Mesoporous Silica Using Light-Induced Sol-Gel Chemistry

*Johanna Gluns, Lucy Zhao, Dieter Spiehl, Joanna J. Mikolei, Raheleh Pardehkhorram, Marcelo Ceolin, and Annette Andrieu-Brunsen**

Mesoporous ceramic materials used in applications such as catalysis, filtration, or sensing, are usually hierarchically structured. Thereby, their structural hierarchy is often inherently related to the manufacturing methods and cannot be independently locally designed along all length scales. This study combines light-based additive manufacturing and bottom-up light-induced self-assembly (LISA) sol-gel chemistry to engineer hierarchically structured porous silica from the nanoscale to the macroscopic object geometry. A LISA-based printing solution that enables printing of ordered mesoporous silica with geometrically complex shapes by using a commercially available digital light processing (DLP)-based 3D printer is presented. This approach exploits the self-assembly process of block copolymer mesopore templates, such as Pluronic P123, and hydrolysis and condensation of silica precursors upon irradiation in the 3D printer to shape mesoporous silica objects. Furthermore, different resins are added to the LISA solution to print 3D silica-resin objects. Mesoporous silica objects up to 10 mm in size, consisting of ordered mesopores with diameters around 5 nm and having high specific surface areas of ≈400 m^2 g^{-1} are successfully printed with a fast and easy post-processing.

1. Introduction

Mesoporous silica is of interest in applications, such as separation,[1] filtration,[2] and catalysis.[3] Its application is based on its tunable pore size,[4] high thermal stability,[5] large accessible surface area, and high concentration of surface species that allow further modifications.[6] So far, shaping of mesoporous silica is dictated by its synthesis methods. For example, synthesis of mesoporous silica nanospheres,[7] nanoparticles[8] or thin films by dip-coating, spray-coating[9,10] or gravure printing[11] have been established. While the evaporation-induced self-assembly process (EISA) is mostly used for the preparation of mesoporous thin films, its industrial-scale implementation is complicated by the need for large amounts of solvents to evaporate, and high temperature requirements during complex post-processing steps.[9,10,12] An alternative approach to prepare mesoporous silica films is the light-induced self-assembly process (LISA). LISA substitutes evaporation in EISA with UV light as the trigger for self-assembly of the amphiphilic block copolymer mesopore template.[13,14] Upon irradiation-initiated photolysis of the photoacid generator (PAG), Brønsted acid which induced hydrolysis and condensation reactions of the silica precursor was released.[15] This resulted in a polarity change of the LISA solution which induced the self-assembly process of the mesopore template.[14] Different solution compositions and thin film preparation conditions, have been systematically studied regarding the obtained mesostructures using LISA.[16,17] To make LISA environmentally friendly, LEDs were employed as light source by adding photosensitizers (PS) to the LISA solution that shifts the active wavelength towards visible light, matching the LED emission.[15] Nevertheless, geometries of to date reported mesoporous silica objects are still limited to films or particles. In addition to the nanoscale structure, the macroscopic shaping of the mesoporous material is relevant for the desired application as it directly impacts the mechanical strength, mass transport, structural integrity and handling properties, for example.[18] 3D printing, also known as additive manufacturing (AM), has attracted increasing attention in the recent years, since it represents a fast, precise and customized solution for fabricating geometrically demanding

J. Gluns, L. Zhao, D. Spiehl, J. J. Mikolei, R. Pardehkhorram, A. Andrieu-Brunsen
Ernst-Berl Institut für Technische und Makromolekulare Chemie
Makromolekulare Chemie - Smart Membranes
Technische Universität Darmstadt
Peter-Grünberg-Str. 8, D-64287 Darmstadt, Germany
E-mail: annette.andrieu-brunsen@tu-darmstadt.de

D. Spiehl
Institut für Druckmaschinen und Druckverfahren - IDD
Technische Universität Darmstadt
Magdalenenstr. 2, D-60289 Darmstadt, Germany

M. Ceolin
Instituto de Investigaciones Fisicoquímicas Teóricas y Aplicadas
Universidad Nacional de La Plata and CONICET
Diag. 113 y 64, La Plata B1900, Argentina

The ORCID identification number(s) for the author(s) of this article can be found under https://doi.org/10.1002/adfm.202405511

DOI: 10.1002/adfm.202405511

objects, including those consisting of multiple materials.[19] Additional advantages of AM include potential for reduced material usage and waste generation.[20,21] Various materials are nowadays being processed using 3D printing, including ceramics.[22,23] In particular, porous ceramics attain interest as they have high potential for applications such as tissue engineering[24,25] and catalyst support.[26] The produced porous ceramics structures should ideally possess precisely customized architectures with structural control of porosity, pore size, pore interconnectivity for optimized applications.[25] Ceramics have been printed by direct ink writing (DIW), selective laser sintering (SLS) or digital light processing (DLP) among many other printing technologies using either ceramic powders, ceramic slurries containing photopolymerizable monomers, or higher viscous ceramic pastes.[27] Recent studies presented DIW to macroscopically shape porous silica while tailoring the porous network by using the EISA approach. However, due to the evaporation process time-consuming post-processing procedures were necessary.[28,29] Large amounts of solvents for evaporation also caused significant shrinkage of the printed object, which complicates the macroscopic structural control.[28] The DIW process itself limits the printing of 3D objects to the mm-to µm-range by the use of a nozzle and in addition limits the shape to lattice-based structures.

So far, the highest resolution and complex structures were achieved by light-based 3D printing technologies as compared to conventional 3D printing technologies. Light-based 3D printing technologies are versatile in terms of equipment setup and material requirements.[21,22,30] For example, the latest printing technology using two-photon polymerization (TPP) enables an improved lateral resolution of ≈100 nm.[22] These high-resolution produced objects printed using TPP are restricted to small sizes on the micrometer scale[31] and the printing process requires relatively long production times due to the high precision.[22] In general, the higher the desired precision and the larger the printed object, the longer the printing time. Despite technical advances in 3D printing, this resolution is not sufficient for directly printing mesopores (with pore diameters of 2 to 50 nm[32]). Due to the size restriction of TPP-based 3D printing, new processes to produce hierarchical structures on a nanometer to meter scale are necessary to develop novel materials with specific properties, such as superhydrophobic surfaces or anisotropic transport.[31] Although DLP provided the highest macroscopic printing accuracy for ceramics, this technique limits the ceramic powder loading in the ink as light may be scattered, thus reducing the possible resolution.[21] For example, Kotz et al. demonstrated that printing of non-porous, transparent silica with high resolution was enabled by using an optimal index-matched monomer-particle ink consisting of a relatively high concentrated dispersion of 35 vol% nanoparticles in a polymerizable monomer.[33] Consequently, in order to exploit the achievable high resolution and design flexibility provided by light-based 3D printing, new printing solutions have been developed to macroscopically shape silica without the use of nanoparticles. To date, DLP[34–36] and TPP[37] were successfully used to print silica. For this purpose, so-called hybrid ceramic precursors in combination with other conventional precursors for sol-gel chemistry were used to either print transparent fused silica glass[34] or dense 3D objects with high silica content.[35] This included tetramethyl orthosilicate (TMOS), trimethoxymethylsilane (MTMS) or tetraethyl orthosilicate (TEOS).[34,35] In this context 3-acryloxypropyl trimethoxysilane (APTMS) was used as a so-called hybrid precursor, containing a carbon–carbon double bond to participate in the radical polymerization, and methoxy groups bonded to the silicon atom which undergoes hydrolysis and condensation in the sol-gel process. As the radical polymerization resulted in shape formation upon irradiation within seconds, the slower hydrolysis and condensation mainly occurred during the temperature increase of the post-treatment.[35] Another approach to obtain high level of control on shape formation during light-based 3D printing of silica was based on the photopolymerization-induced phase separation of so-called hybrid printing solutions.[36] This so-called hybrid printing solution consisted of an alkoxide inorganic precursor such as poly(diethoxysiloxane) (PDEOS) that needed trimethyl borate (TMB) for polycondensation, mixed with photoreactive monomers, such as urethane acrylate (UA, as commercially available resin U25-20D) and tripropyleneglycol diacrylate (TPGDA), undergoing a radical polymerization following activation of a photoinitiator by irradiation. The as-printed polymer-silica hybrid material was calcined to remove the radically polymerized polymer leaving an unordered porous structure with voids in the range of 210–320 nm. Subsequent sintering of the porous structures led to dense, transparent multicomponent glasses.[36] A so-called hybrid printing solution with the advantage of combining fast radical polymerization and slower hydrolysis and condensation-based sol-gel chemistry, was also exploited in a recent study of Shukrun et al. to produce complex 3D mesoporous silica objects.[38] The presented printing solution consisted of TEOS as silica precursor, Pluronic F127 as mesopore template and an elastomer-forming ink that contained a monomer which was photocurable by radical polymerization. Upon irradiation, the photocurable monomer solidified due to its radical polymerization and thus entrapped the sol-gel solution within the formed polymer network. The mesopore formation process took place subsequently in a one week aging process under controlled environmental conditions while the solvent evaporated.[38] A silica network shrinkage of 12 ±5 vol% was observed after the aging process. The obtained polymer-silica object contained ≈10 wt% silica. Subsequent calcination of the as-printed hybrid polymer-silica object resulted in the removal of the stabilizing polymer network and the mesopore template generating a 3D macroporous silica object containing ordered mesopores with an average pore size of ≈5.7 nm. An isotropic shrinkage of 62 ±1 vol% was observed as a result of the calcination step. Mesoporous silica objects in different 3D shapes with sizes up to 1.5 cm were successfully printed.[38] When replacing the photocurable monomer, which forms a stabilizing polymer scaffold during light-based 3D printing, with the hybrid precursor APTMS, the printed silica objects needed to undergo a complex post-treatment consisting of solvent exchanges and super critical drying (SCD) to obtain mesopores. This is the case because no mesopore forming template was used.[37] By using this SCD process mesopores were formed in an uncontrolled manner showing a broad distribution of pore diameters between 2–120 nm and thus ranging from meso- to macropores. A direct approach to print 3D shapes of mesoporous silica with controlled pore sizes was presented by Aubert et al. using synthesized, prefunctionalized silica nanocages with a size of 10 nm

Table 1. Summarized printing parameters for different LISA-resin solutions (LISA-SKresin 1:1 vol/vol, LISA-Liqcreate 1:1 vol/vol, LISA-Liqcreate 2:1 vol/vol).

Parameters	Unit	LISA-SKresin 1:1 vol/vol	LISA-Liqcreate 1:1 vol/vol	LISA-Liqcreate 2:1 vol/vol
Light intensity	mW cm^{-2}	5	5	5
Irradiation time (BL)	S	24	60	60
Irradiation time (NL)	s	12	24	24
Layer thickness	µm	40	40	40
Waiting period after irradiation (BL)	s	0.25	2	2
Waiting period after separation (BL)	s	20	20	20
Waiting period after irradiation (NL)	s	0.25	0.1	0.1
Waiting period after separation (NL)	s	10	20	20
Approach velocity	mm s^{-1}	2.48	2.48	2.48
Separation velocity	mm s^{-1}	4.30	4.30	4.30

((BL) = bottom layer, meaning the first two layers in the shown printed objects, (NL) = normal layer).

as photocurable monomers in a radical polymerization in a DLP-based printer.[39] Despite the substantial fundamental and technological interest in defined design of hierarchically porous ceramic materials from the nanoscale porosity to macroscopic object size, controlled mesopore formation during light-based 3D printing process has not been demonstrated yet. Mesopore formation is not independently controlled and when increasing control on nanoscale pore formation, post-processing steps require days up to a week.

In this study, 3D printing of ordered mesoporous silica with high specific surface area was achieved by using a LISA-based printing solution containing a self-assembling mesopore template, in a commercial DLP-based 3D printer. Various, geometrically complex, ordered mesoporous silica objects up to 10 mm in size were printed. The light-induced self-assembly process enables a controlled mesopore formation upon irradiation, at which the silica precursor in the LISA solution undergoes hydrolysis and polycondensation to form the silica network. Hierarchically structured 3D objects were obtained when mixing the LISA solution with a photocurable resin, which enables fast solidification and envisions to provide an additional control in the micrometer range of the printed object upon calcination. Thus, hierarchically porous silica in different shapes such as gyroids with defined structures in nano-, micro- and macroscale with high specific surface areas can be printed requiring only short and simple post-processing.

2. Results and Discussion

3D printed mesoporous silica objects with adjustable shape were obtained using the LISA process, allowing mesoporous silica formation upon light irradiation in combination with a photocurable resin, SKresin 1330 (referred to as SKresin) or Liqcreate Premium Flex (referred to as Liqcreate), supporting fast curing during irradiation (**Figure 1**). The optimized conditions finally used for 3D printing are summarized in **Table 1**. To optimize the adhesion to the stage, longer waiting periods for the bottom (first to be printed) layers proved to be useful. The as-printed objects contained the polymer originating from the radical polymerization as well as the mesopore template Pluronic P123 from the LISA process. Both were removed within a post-printing thermal calcination step by heating the object up to 600 °C for up to 16 h in total. After calcination, the 3D mesoporous objects consisting of pure silica were obtained. Thereby, the chemical composition was analyzed using ATR-IR spectroscopy, and structural properties were characterized by SEM, TEM, SAXS and gas adsorption measurements.

To print 3D mesoporous silica objects with various shapes, the LISA solution was combined with different commercially available, radically polymerizing resins to speed up the printing process and to improve the precision in shape formation. SKresin and Liqcreate were selected due to their fast solidification and their miscibility with the LISA solution. The flexibility of the Liqcreate polymer network is expected to be beneficial for maintaining a stable shape of the mesoporous silica object during the calcination step causing polymer removal and simultaneous silica network shrinkage. The idea to use an elastomer-forming ink was inspired by Shukrun Farrell et al.[38] Both ink compositions were investigated regarding their printability as well as their precision of shape formation at the micrometer (**Figures 2** and **3**) and at the nanometer scale (Figure 3). Cuboid and cylinder objects were printed, respectively (Figures 2 and 3).

For both LISA-resin solutions, cuboids and cylinders were successfully printed (Figure 2a,d). The presence of silica and the respective resin in the as-printed objects was confirmed by ATR-IR spectroscopy (Figure S1a,b, Supporting Information). Printing in presence of the SKresin (Figure 2a–c) shows a higher object stability throughout the printing process as compared to the Liqcreate containing LISA solution (Figure 2d–f). This is mainly ascribed to the more rigid structure of the silica-SKresin object and the stronger adhesion of the printed object to the stage. On the other hand, the objects printed in presence of the Liqcreate resin contain a slightly higher relative mass of silica of 19.8 ±0.2 wt% as compared to 16.3 ±0.2 wt% for the object printed using the LISA-SKresin solution (Figure S2, Supporting Information). This obtained silica content is higher than the ≈10 wt% reported in literature for 3D printed mesoporous silica objects.[38] The lateral size of the silica-SKresin objects is only slightly, up to 2%, smaller than intended. This deviation corresponds to up to 0.13 mm for objects with dimensions from 5

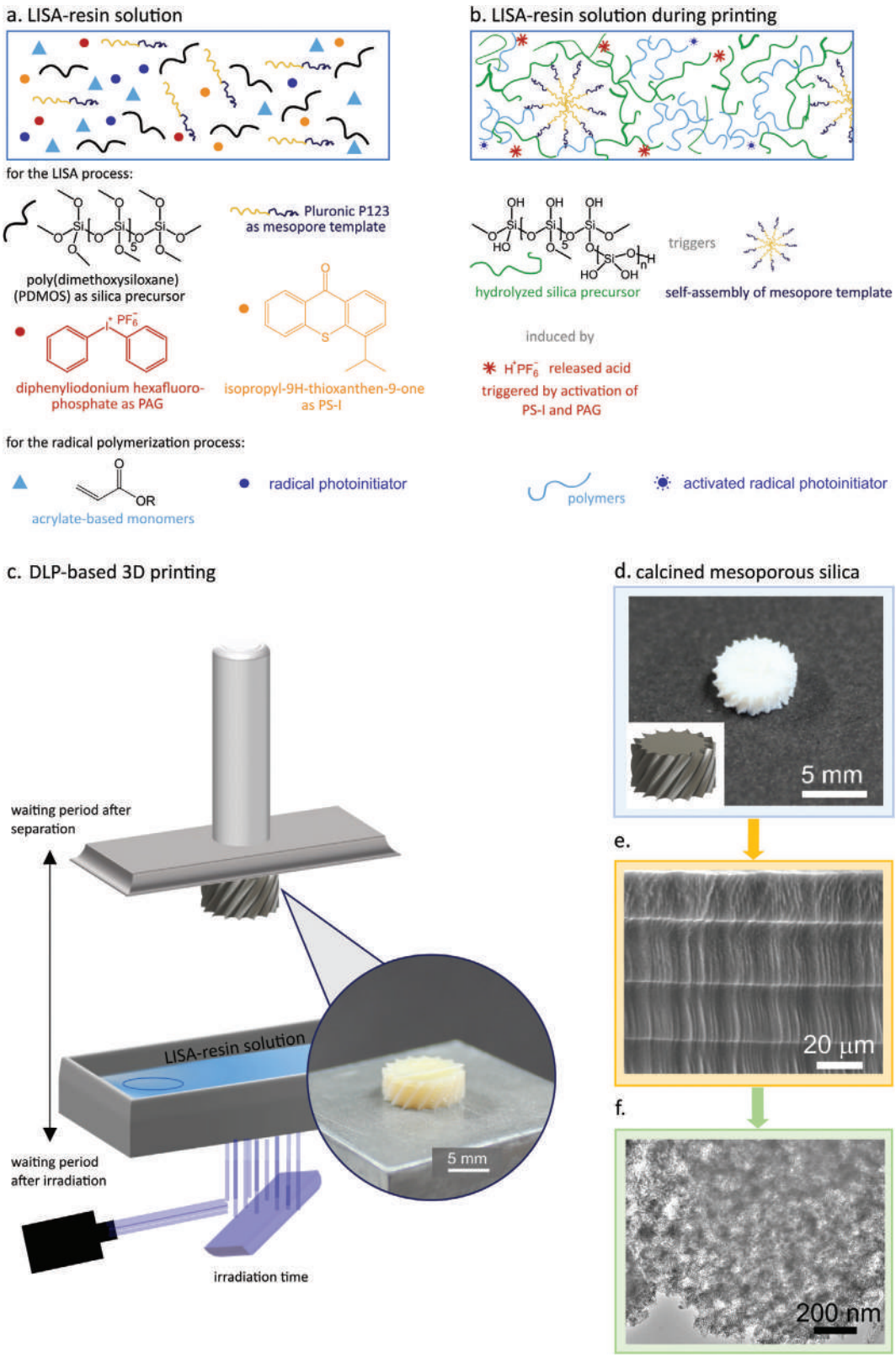

Figure 1. a) The LISA-based printing solution contains following components: silica precursor, PAG, PS-I, mesopore template, the commercial acrylate-based resin which includes a radical photoinitiator, and solvents. b) Schematic illustration of the LISA process during c) 3D printing. The printed, solid LISA-resin object is then d) calcined to obtain the mesoporous silica object (blue) and hereby controlling e) the material architecture on µm- (SEM image, yellow) and f) nm-scale (TEM image, green). This schematic illustration of the process may vary upon printing solution composition and is therefore for general understanding only.

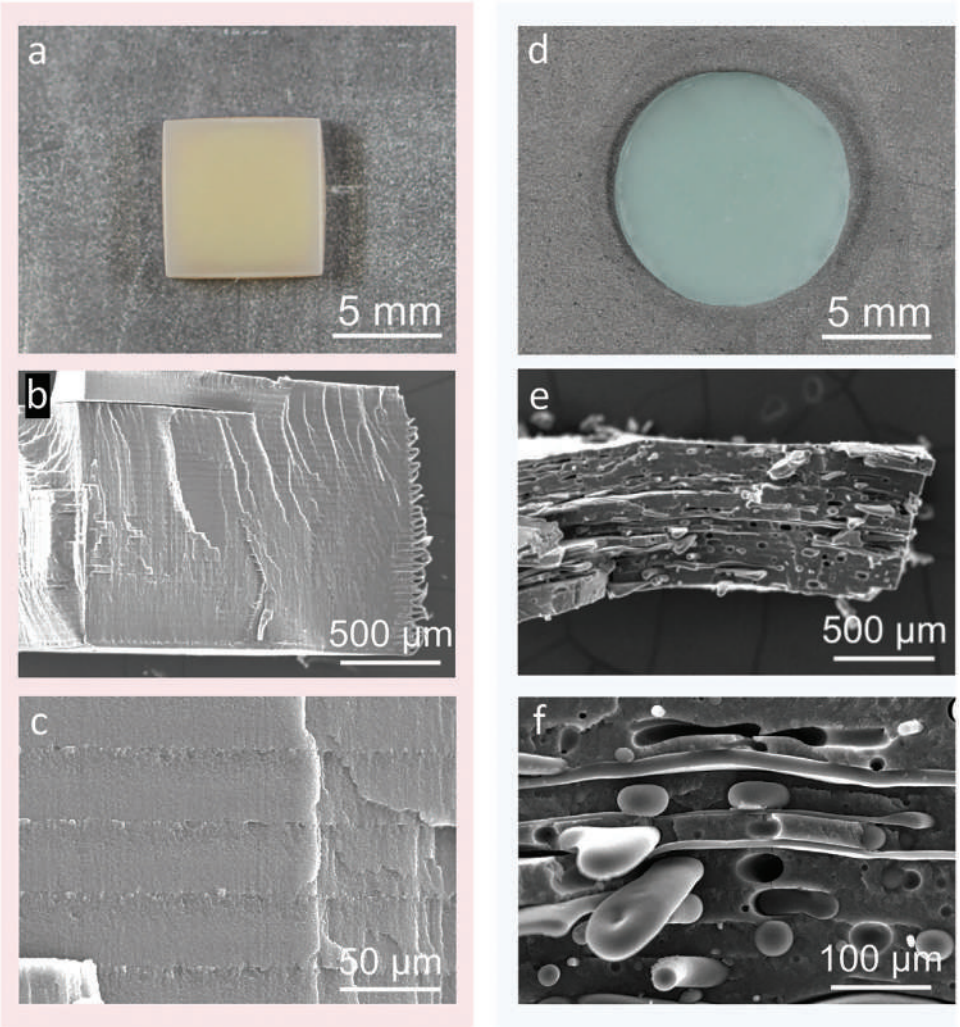

Figure 2. a) 3D printed silica object using the LISA-SKresin solution (red): b) cross-section SEM image and c) its magnified view. d) 3D printed silica object using the LISA-Liqcreate solution (blue): e) cross-section SEM image and f) its magnified view.

to 10 mm. Silica-Liqcreate objects exhibit a lateral size deviation of 1–5% compared to the designed model which corresponds to 0.1–0.4 mm for objects with dimensions in the range of 5–10 mm. The thickness of each printed layer is 36.4 ±0.6 µm for silica-SKresin objects (Figure 2b,c). Thus, the experimentally determined layer thickness is 9% smaller than the intended thickness of 40 µm specified in the printing process. A similar layer thickness reduction of about 12% resulting in a layer thickness of 35.4 ±2.1 µm was determined for silica-Liqcreate objects (Figure 2e,f). The comparison of the printed objects using LISA-SKresin and LISA-Liqcreate solutions leads to the conclusion that the slightly higher amount of silica in the printed object entails a higher deviation of lateral size and layer thickness from the designed shape. Magnified SEM images of silica-SKresin objects show homogeneous layers (Figure 2c). It has to be noted that silica-Liqcreate objects reveal separated volumes of solidified commercial resin and silica as indicated by voids being 4–69 µm in width and 3–33 µm in height (Figure 2f). This separation of resin and silica may as well explain the lower layer stability of silica-Liqcreate objects as compared to silica-SKresin objects during the printing process. To obtain mesoporous silica the printed objects were thermally treated at 600 °C for 2 h (Figure 3).

The shape of the calcined mesoporous silica cuboid prepared using the LISA-SKresin solution remained stable upon calcination (Figure 3a). It has to be noted that a few cracks on the surface occurred. The lateral size of the printed silica-SKresin objects decreases by 30% upon calcination and the layer thickness reduces by 30% from 36.4 ±0.6 to 25.5 ±0.9 µm (Figures 2c and 3b). As the silica-Liqcreate object contains segregated resin in the micrometer scale, the removal of Liqcreate has contributed to the destruction of the object shape on the macroscopic scale (Figure 3f). A layer shrinkage from 35.4 ±2.1 to 32.5 ±1.4 µm by 8% was determined (Figures 2f and 3g). Since both resins are incorporated differently in the silica-resin object, different voids remain upon resin removal, allowing to tune the µm-scale porous structure by selecting the resin (Figure 3b,g and Figure S3a–d, Supporting Information). The calcination of a silica-SKresin object results in a silica object containing voids of 0.8-2.6 µm (Figure 3b). Calcination of a silica-Liqcreate object yields a silica object containing

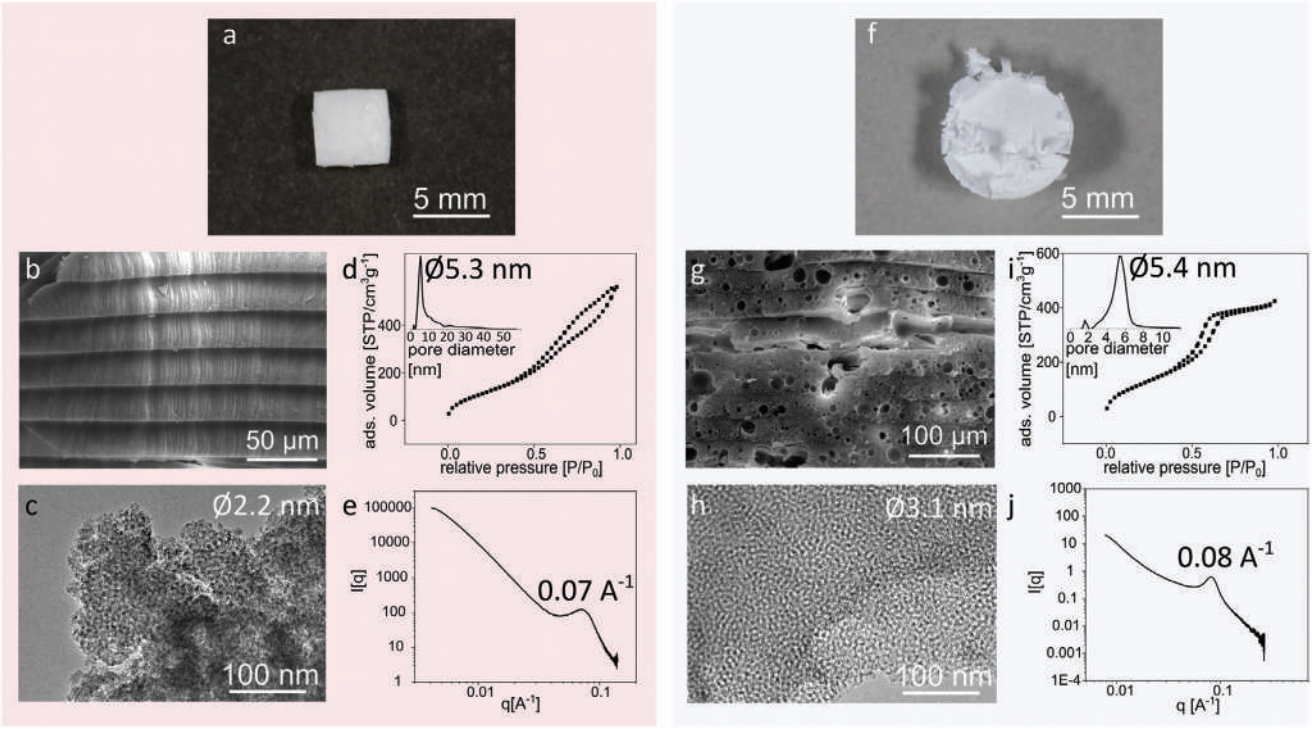

Figure 3. a–e) 3D printed silica object using the LISA-SKresin solution after calcination at 600 °C: b) cross-section SEM image, and c) TEM image of the calcined silica object averaging Ø116 pores to determine the pore diameter, d) argon gas adsorption isotherm and determined pore diameter distribution, and e) SAXS measurement. f–i) 3D printed silica object using the LISA-Liqcreate solution after calcination at 600 °C: g) cross-section SEM image, h) TEM image of the calcined silica object averaging Ø103 pores for pore diameter determination, i) argon gas adsorption isotherm and deduced pore diameter distribution, j) SAXS measurement.

larger voids of 2–23 µm in size (Figure 3g). Besides the µm-sized voids, these calcined silica objects are mesoporous as deduced from the TEM images (Figure 3c,h and Figure S4, Supporting Information). Mesoporosity is additionally confirmed by argon adsorption measurements showing an adsorption–desorption isotherm with a hysteresis loop (Figure 3d,i). The isotherm of the mesoporous silica object printed using the LISA-SKresin solution (Figure 3d) indicates the presence of macropores due to the lack of a saturation behavior at a relative pressure of ≈1. According to literature,[40] the isotherm of the mesoporous silica object printed using the LISA-Liqcreate solution can be specified to a type IV(a) isotherm with a H1 hysteresis loop (Figure 3i), which is often found in mesoporous materials with uniform cylindrical pore or ordered 3D pore networks. Furthermore, a small amount of micropores (pore diameters <2 nm[32]), can be deduced from the small pressure range (Figure 3d,i and Figure S5a,b, Supporting Information).[40a] An average mesopore diameter of 2.2 nm of the silica object originating from the silica-SKresin object is determined by TEM (Figure 3c), while argon gas adsorption measurement suggests mesopores with an average pore diameter of 5.3 nm (±1.2 nm) (Figure 3d). According to argon gas adsorption measurement, the printed mesoporous silica using the LISA-SKresin solution possesses a high specific surface area of 399 m^2 g^{-1} (R = 0.99963). Furthermore, SAXS measurement of the mesoporous silica object printed using the LISA-SKresin solution reveals ordered mesopore formation (Figure 3e). The mesopores acting as scattering centers are arranged in a regular distance of 9.0 nm as deduced from the Bragg Peak at 0.07 A^{-1} in the SAXS measurement (Figure 3e). A crystalline domain size of 36 nm was calculated using the Scherrer equation.[41] By printing with the LISA-Liqcreate solution, an average pore diameter of 3.1 nm according to TEM (Figure 3h), and 5.4 nm (±0.8 nm) according to argon gas adsorption measurement was obtained (Figure 3i). As visible in the TEM image, the mesoporous silica object obtained after silica-Liqcreate object calcination consists of wormlike mesopores (Figure 3h). Mesoporous silica obtained using the LISA-Liqcreate solution as well exhibits a similar high specific surface area of 416 m^2 g^{-1} (R = 0.99978). Similar distances between mesopores of 7.6 nm in domains of 43 nm in size were detected using SAXS (Figure 3j).

Consequently, combining a LISA solution with commercial resin to print 3D silica-resin objects resulted in 3D, ordered mesoporous silica objects with high and ordered mesopore volume and high specific surface areas after calcination. Both printed mesoporous silica objects have similar pore diameters, distances between the mesopores and domain sizes, independently of the resin that was used. This observation suggests that the resins chosen here do not have a significant influence on the LISA-based mesopore formation process. The addition of the resin to the LISA solution enabled fast printing, shape accuracy and macroporous voids after resin removal. This approach provides the opportunity to control the pores or voids in the nm- and µm-scale by two separate mechanisms in a light-based 3D printing process.

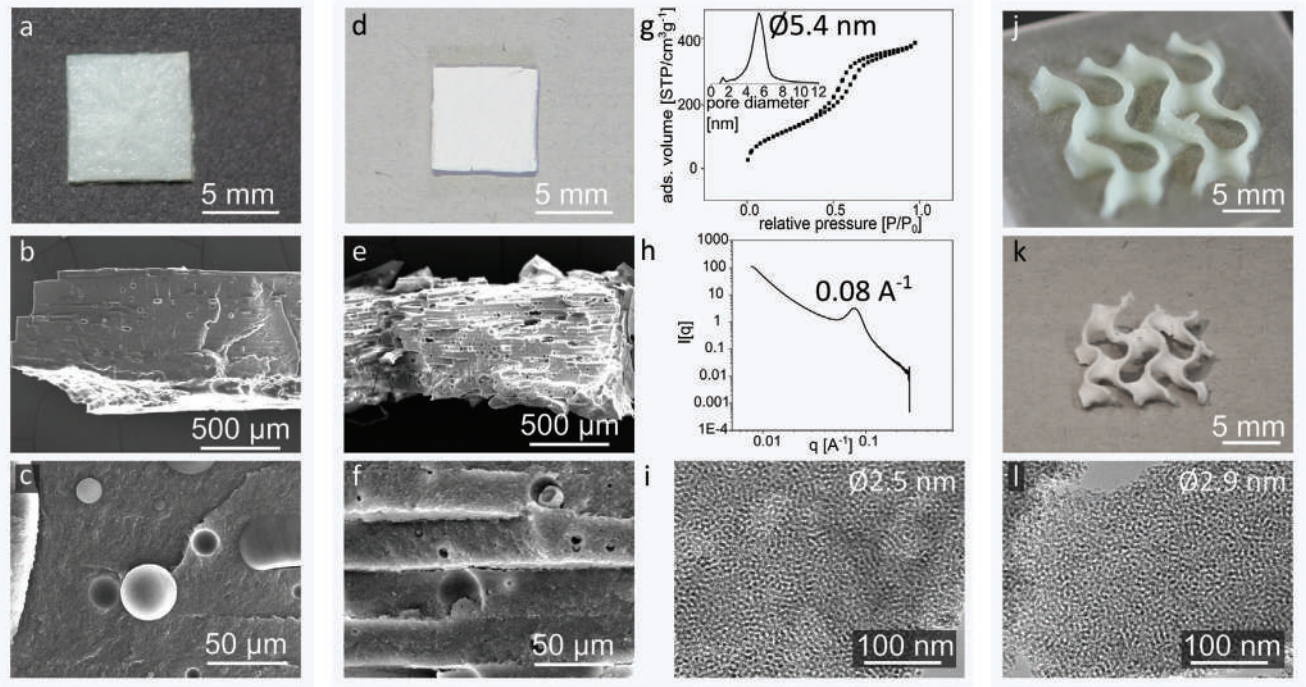

Figure 4. a–c) 3D printed silica object using the LISA-Liqcreate solution (2:1 vol/vol) before calcination: b) cross-section SEM image and c) its magnified view, and d–i) after calcination at 600 °C: e) cross-section SEM image and f) its magnified view, g) argon gas adsorption isotherm and determined pore diameter distribution, h) SAXS measurement, i) TEM image averaging Ø100 pores to determine the pore diameter. j) Image of a printed interconnected wavy object using the LISA-Liqcreate solution (2:1 vol/vol) before and k) after calcination, with l) TEM analysis to determine the pore diameter by averaging Ø100 pores.

The silica amount in the printed object can be further increased by adjusting the LISA:Liqcreate ratio from 1:1 vol/vol to 2:1 vol/vol (**Figure 4**).

For example, silica-Liqcreate objects in the shape of a cuboid, were successfully printed (Figure 4a), with the hybrid composition confirmed by the ATR-IR spectrum (Figure S1c, Supporting Information). A silica content of 27.4 ±0.1 wt% was achieved which is 1.4 times higher as compared to the LISA-Liqcreate solution (1:1 vol/vol) (Figure S2, Supporting Information). The silica cuboid with a size of 8.1 ±0.1 mm was printed deviating only 2% from the intended size of 8 × 8 mm before calcination (Figure 4a). The thickness of each printed layer was determined to be 31.6 ±1.9 µm which is 21% thinner as the intended value of 40 µm (Figure 4b). Furthermore, less separation of resin voids and silica is observed compared to the results before from 1:1 vol/vol LISA-Liqcreate solution, as deduced from SEM images (Figures 2f and 4b and Figure S3e,f, Supporting Information). The remaining resin containing voids are 2–75 µm in width and 2–30 µm in height (Figure 4b,c). As the number of separated, resin filled voids was reduced, the calcination of the printed object led to a more homogeneous structure as compared to the structure when using the 1:1 vol/vol LISA-Liqcreate solution. As well the stability upon calcination is improved as the silica cuboid shows a significantly reduced number of cracks on the surface (Figure 4d). Calcination led to lateral shrinkage of 22% from 8.1 ±0.1 to 6.3 ±0.3 mm and a layer thickness reduction of 13% from 31.6 ±1.9 to 27.9 ±1.2 µm (Figure 4b,e). The voids created by the Liqcreate removal upon calcination are 2–51 µm in width and 3–30 µm in height (Figure 4e,f). Consequently, reducing the resin content leads to increasing silica amount in the silica-resin containing object from a relative mass of 19.8 to 27.4 wt% (Figure S2, Supporting Information) and a reduced individual layer thickness of ≈3.8 µm which represents an increased deviation from the intended layer thickness from 12% to 21% upon reducing the resin amount (Figures 2f and 4b). Mesopore diameters and specific surface area remain nearly identical between both resins independently of the increased silica content in the LISA solution. Furthermore, a very small quantity of micropores is also detected during gas adsorption measurement of the printed mesoporous silica object printing with the LISA-Liqcreate solution (2:1 vol/vol) (Figure 4g and Figure S5c, Supporting Information). A specific surface area of 393 m^2 g^{-1} (R = 0.99989), an average pore diameter of 2.5 nm in TEM and an average pore diameter of 5.3 nm (±0.8 nm) in argon gas adsorption measurement were detected for the mesoporous silica object prepared using the LISA-Liqcreate solution with the volume ratio 2:1 (Figure 4g,i and Figure S6a, Supporting Information). The obtained ordered mesopores are arranged in a regular distance of 8.0 nm and in domains of 41 nm in size (Figure 4h), which are in good agreement with these properties obtained using the LISA-Liqcreate solution (1:1 vol/vol) (Figure 3j). This indicates that the mesopore formation of the LISA solution is not influenced by the amount of resin or the geometric shape of the printed object. In agreement with previous results on printed mesoporous silica cuboids (Figure 4d), a mesoporous interconnected wavy shaped silica object is obtained after calcination showing an average pore

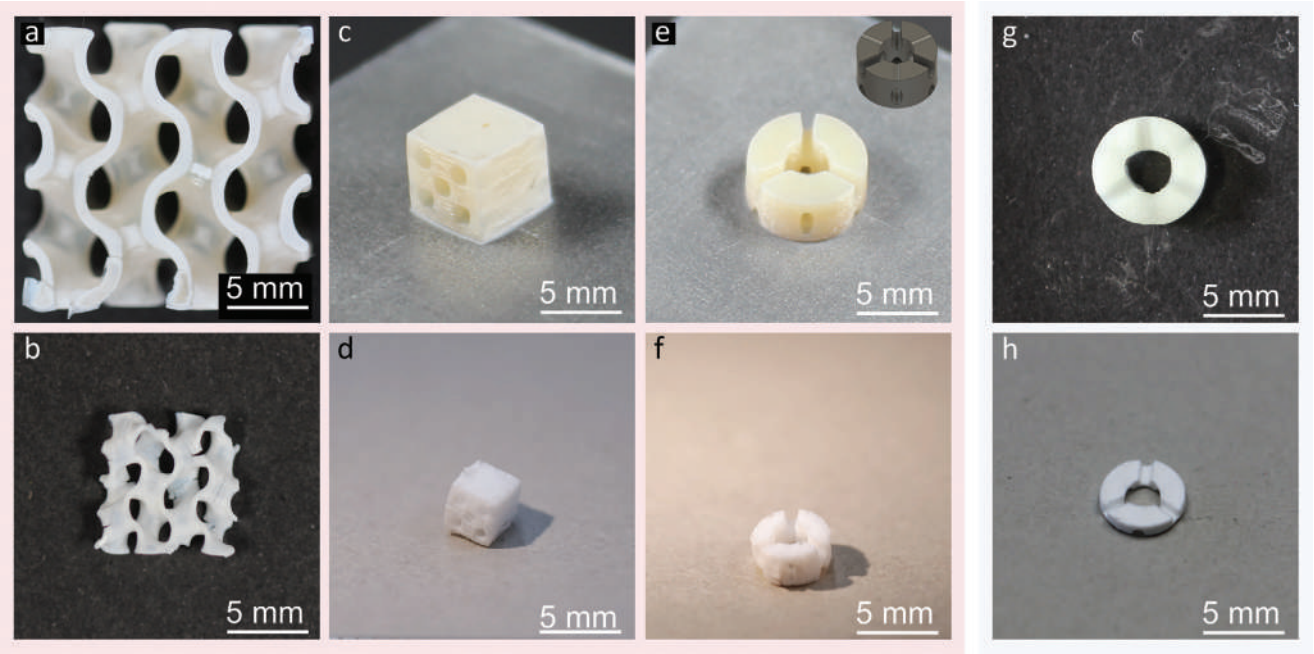

Figure 5. 3D printed silica objects using the LISA-SKresin solution a,c,e) before and b,d,f) after calcination: a,b) gyroid, c,d) cuboid with holes, e,f) hollow column (zoom-in: CAD model). 3D printed silica hollow column using the LISA-Liqcreate solution (2:1 vol/vol) g) before and h) after calcination.

diameter of 2.9 nm according to TEM images (Figure 4k,l and Figure S6b, Supporting Information).

In addition to relatively simple silica object geometries, printing of alternating overhangs and connected areas using LISA in combination with SKresin or a reduced amount of Liqcreate resin was realized (**Figure 5**).

Furthermore, printing wall thicknesses from 0.2-0.8 mm was demonstrated by printing 15 mm long lines using the LISA-SKresin solution (Figure S8a,b, Supporting Information). It has to be noted that single lines were not stable upon calcination under the applied conditions (Figure S8c, Supporting Information) while self-supporting, calcined mesoporous silica objects such as gyroid, cuboids with holes or hollow columns were stably produced (Figure 5b,d,f,h). As the TEM and SAXS data confirm, mesoporous silica was also obtained after the calcination process of these complex shapes (Figure S7, Supporting Information). Comparing mesopore diameters, domain sizes and pore arrangements reveal that changing the macroscopically printed object shape does result in similar structural properties with respect to the mesoporous structure.

Thus, it has been shown that LISA-SKresin and LISA-Liqcreate (2:1 vol/vol) solutions can be both printed into complex shapes using a commercial 3D printer (Figure 5 and Figure S9, Supporting Information). This is especially relevant with respect to applications, such as separation or catalysis, which benefit from complex geometries, such as gyroids with respect to optimized mass transfer and mixing while providing high surface areas.[42]

3. Conclusion

We present the first example of 3D printing of ordered mesoporous silica using light-induced sol-gel chemistry and a commercially available 3D printer. Combining bottom-up LISA for mesoporous silica formation with resins that are able to undergo radical polymerization and 3D printing allows to print complex 3D mesoporous silica objects with an ordered mesoporous structure. Thereby, the combination of LISA and DLP-based 3D printing is intended to enable the control of structure formation from the mesopore nanometer length scale via the micrometer to the macroscopic object length scale. Since the hydrolysis and condensation reaction of the alkoxy silica precursor, the mesopore forming template assembly, and the radical polymerization of the resins take place simultaneously upon irradiation in the printing process, no time-consuming post-treatment ensuring mesopore formation is required. After the removal of mesopore template and the polymer network originating from the resin, ordered mesoporous silica objects with pore diameters of approximately 5 nm with high specific surface areas of ≈400 m^2 g^{-1} were obtained. Future work will be dedicated to increase the resolution of the printed objects through the use of, e.g., TPP-based high resolution 3D printers. Furthermore, this approach should be compatible with co-condensation[43] or with the use of functional mesopore templates[44] for in situ polymer functionalization to generate a variety of functionalized mesoporous silica objects with application-oriented geometries in future studies. Thinking ahead, multifunctional, hybrid mesoporous silica objects can be created by using different printing solutions in a multi-material printer setup.[45] The opportunity to design the shape of the possibly functionalized, mesoporous silica object is envisioned to open new possibilities for future applications, such as filtration, separation, drug delivery, or catalysis.

4. Experimental Section

Chemicals: All chemicals and solvents were purchased from Sigma Aldrich, Merck, VWR, Alfa Aesar, abcr, and used as received unless stated

otherwise. The solutions for the LISA process were prepared with PDMOS (abcr) as silica precursor, Pluronic P123 (average $M_n \approx 5800$ g mol^{-1}, Sigma Aldrich) as mesopore template, diphenyliodonium hexafluorophosphate (Alfa Aesar, 98%) as PAG, isopropyl-9H-thioxanthen-9-one (Sigma Aldrich, 97%) as PS-I, technical grade of methanol and toluene (VWR, ≥98%) and distilled water. *SKresin 1330*, referred to as SKresin, was provided by S u. K. Hock GmbH and *Liqcreate Premium Flex*, referred to as Liqcreate, was purchased from Liqcreate. For TEM sample preparation Emplura ethanol (≥99.5%, Merck) was used.

LISA Solution Preparation: The LISA solution composition was originally adapted from literature[15,17] and already used in the previous study to print mesoporous silica shapes.[46] The LISA solution contained the following components PDMOS:Pluronic P123:PAG:PS-I (1:0.0075:0.0075:0.02 molar ratio) and 30 wt% methanol : toluene (3:1 vol/vol) based on PDMOS. For preparing the LISA solution PDMOS, Pluronic P123 and the solvent mixture were treated together in an ultrasonic bath for 10 min, before PAG and PS-I were added. This solution was kept in the dark while stirring over night at ambient temperature. Until use, this solution was stored in the freezer (−18 °C).

Printing: The printing process took place under UV-free yellow light (no irradiation below 470 nm wavelength). The LISA solution (1 mL or 2 mL per print) was mixed with the commercial resins in different volumetric ratios (vol/vol) and stirred for 5 min. The LISA-resin solution was kept in the dark during stirring. Subsequently, 1 vol% of distilled water related to the LISA solution volume was added and stirred for 5 min. Then the LISA-resin solution was poured into the vat of the 3D printer (Asiga MAX X27 equipped with 385 nm LED, Sydney, Australia). This printer has a printing resolution of 27 µm per pixel. To start the 3D printing process the stage was moved down into the solution, hereby adjusting the thickness of the individual layer. Then, irradiation was followed by a first waiting period after irradiation, before moving the stage back up. Subsequently, a second waiting period under ambient conditions in contact with air was added after separating the stage from the ink solution. These individual process steps were adjusted for each ink composition. The optimized printing parameters for the respective LISA-resin solution is summarized in Table 1. The number of layers varied for each printed object. For example, the cuboid shown in Figure 2a consisted of 58 normal layers and 2 bottom layers, while the cylinder shown in Figure 2d consisted of 23 normal layers and 2 bottom layers. As the process was set for printing each individual layer, the total printing time depended on the number of layers. For example, the total printing times for the objects shown in Figures 2a,d and 5a,g were 42 min, 28 min, 56 min, and 46 min, respectively. After the print job finished, the silica-resin object was carefully rinsed with toluene to remove the excess solution and gently blown dry. Finally, the silica-resin object was removed from the stage. After a resting time overnight, the silica-resin objects were calcined using an oven program up to 600 °C (ambient temperature, heating up to 480 °C with 1 °C min^{-1}, hold at 480 °C for 4 h, heating up to 600 °C with 1 °C min^{-1} and hold at 600 °C for 2 h, cool down to room temperature).

Transmission Electron Microscopy (TEM): TEM images were recorded using JEOL JEM 2100F transmission electron microscope (Tokyo, Japan) with a maximum resolution of 2 Å operating at an accelerating voltage of 200 kV. Samples were prepared by dispersing in ethanol. After 10 min sonification, a 3.05 mm Cu grid (mesh size 200) with a Lacey carbon film (Plano, Wetzlar, Germany) was dipped into the dispersed solution. With sample covered TEM grid was dried under ambient conditions. The average pore diameter and the pore diameter distribution were determined by averaging at least 100 pores. The measurements of the pore diameters were performed manually using ImageJ.

Scanning Electron Microscopy (SEM): The SEM images were obtained using the Zeiss EVO 10 scanning electron microscope and the software SmartSEM V06.03. (Oberkochen, Germany) with a SE detector, operated at an accelerating voltage of 15–20 kV. The samples were coated with a 10–15 nm coating of Pt/Pd (from ESG Edelmetall-Service, Rheinstetten, Germany) using a Cressington 208 HR sputter coater (Cressington Scientific Instruments sold by TESCAN, Dortmund, Germany).

Argon Gas Adsorption: With argon adsorption at 87 K full isotherms in the relative pressure range from 0 to 1 were measured using an Autosorb iQ (Quantachrome sold by Anton Paar, Ostfildern-Scharnhausen, Germany). Based on the argon gas adsorption isotherms the specific surface area, pore diameter, and the pore diameter distribution were determined using BET (BET; 11 points between 0.05 and 0.3 P/P_0) and the corresponding NLDFT kernel. Before each measurement, the samples were degassed at 80 °C for 12 h under high vacuum.

Small Angle X-Ray Scattering (SAXS): SAXS experiments were performed in a XEUSS 1.0 SAXS setup (XENOCS, Grenoble, France). Monochromatic X-rays ($\lambda = 0.15419$ nm) were produced with a GENIX 3D micro-focus tube. The incoming X-ray beam was collimated to have a size at sample position of 0.5×0.5 mm^2. Scattered photons were detected using a PILATUS 100 K detector placed at $D = 1350$ mm sample to detector distance (calibrated using Silver Behenate as standard). The background (Kapton foil) was subtracted from the SAXS measurements. The crystalline domains were calculated using the classical Scherrer equation.[41] The error quote for the domain size values was estimated to be around 1 nm.

Supporting Information

Supporting Information is available from the Wiley Online Library or from the author.

Acknowledgements

J.G. and L.Z. contributed equally to this work. The authors kindly acknowledge the funding from the European Research Council (ERC) under the European Union´s Horizon 2020 research and innovation program (grant agreement no. 803758). The authors thank Laura Czerwenka for carrying out the gas adsorption measurements. The research group of Prof. Kleebe (Material Science, TU Darmstadt) is acknowledged for access to the TEM. M.C. is a staff member of CONICET Argentina. J.J.M. acknowledges financial support for her research stay at the Instituto de Investigaciones Físicoquimicas Teóricas y Aplicadas (INIFTA-UNLP/CONICET) in La Plata, Argentina by the DAAD (research grand). Furthermore, the authors thank Prof. Azzaroni (INIFTA, La Plata Argentina) for access to the Soft Matter Laboratory facilities and the research group of Prof. Biesalski (TU Darmstadt) for access to their analytic lab for IR, TGA and SEM measurements.

Open access funding enabled and organized by Projekt DEAL.

Conflict of Interest

The authors declare no conflict of interest.

Data Availability Statement

The data that support the findings of this study are available from the corresponding author upon reasonable request.

Keywords

3D printed mesoporous silica, additive manufacturing, DLP, light-induced self-assembly, sol-gel chemistry

Received: March 30, 2024
Revised: May 25, 2024
Published online:

[1] S. Xu, S. Ning, Y. Wang, X. Wang, H. Dong, L. Chen, X. Yin, T. Fujita, Y. Wei, *J. Cleaner Prod.* **2023**, *396*, 136479.

[2] K. Nakagawa, H. Matsuyama, T. Maki, M. Teramoto, N. Kubota, *Sep. Purif. Technol.* **2005**, *44*, 145.
[3] a) X. Yu, C. T. Williams, *Catal. Sci. Technol.* **2022**, *12*, 5765; b) B. Singh, J. Na, M. Konarova, T. Wakihara, Y. Yamauchi, C. Salomon, M. B. Gawande, *Bull. Chem. Soc. Jpn.* **2020**, *93*, 1459.
[4] a) E. Bloch, P. L. Llewellyn, T. Phan, D. Bertin, V. Hornebecq, *Chem. Mater.* **2009**, *21*, 48; b) M. Widenmeyer, R. Anwander, *Chem. Mater.* **2002**, *14*, 1827.
[5] Y. Deng, J. Wei, Z. Sun, D. Zhao, *Chem. Soc. Rev.* **2013**, *42*, 4054.
[6] P. Innocenzi, L. Malfatti, *Chem. Soc. Rev.* **2013**, *42*, 4198.
[7] M. Yu, L. Zhou, J. Zhang, P. Yuan, P. Thorn, W. Gu, C. Yu, *J. Colloid Interface Sci.* **2012**, *376*, 67.
[8] a) R. Narayan, U. Y. Nayak, A. M. Raichur, S. Garg, *Pharmaceutics* **2018**, *10*, 118; b) S.-H. Wu, C.-Y. Mou, H.-P. Lin, *Chem. Soc. Rev.* **2013**, *42*, 3862.
[9] C. J. Brinker, Y. Lu, A. Sellinger, H. Fan, *Adv. Mater.* **1999**, *11*, 579.
[10] D. Grosso, F. Cagnol, G. J. d. A. A. Soler-Illia, E. L. Crepaldi, H. Amenitsch, A. Brunet-Bruneau, A. Bourgeois, C. Sanchez, *Adv. Funct. Mater.* **2004**, *14*, 309.
[11] N. Herzog, R. Brilmayer, M. Stanzel, A. Kalyta, D. Spiehl, E. Dörsam, C. Hess, A. Andrieu-Brunsen, *RSC Adv.* **2019**, *9*, 23570.
[12] L. Nicole, C. Boissière, D. Grosso, A. Quach, C. Sanchez, *J. Mater. Chem.* **2005**, *15*, 3598.
[13] H. de Paz, A. Chemtob, C. Croutxé-Barghorn, S. Rigolet, B. Lebeau, *Microporous Mesoporous Mater.* **2012**, *151*, 88.
[14] H. de Paz-Simon, A. Chemtob, F. Crest, C. Croutxé-Barghorn, L. Michelin, L. Vidal, S. Rigolet, B. Lebeau, *RSC Adv.* **2012**, *2*, 11944.
[15] S. Shi, X. Allonas, C. Croutxé-Barghorn, A. Chemtob, *New J. Chem.* **2015**, *39*, 5686.
[16] H. de Paz-Simon, A. Chemtob, C. Croutxé-Barghorn, S. Rigolet, L. Michelin, L. Vidal, B. Lebeau, *J. Phys. Chem. C* **2014**, *118*, 4959.
[17] M. Sibeaud, H. de Paz-Simon, C. Croutxé-Barghorn, S. Rigolet, L. Michelin, B. Lebeau, L. Vidal, P.-A. Albouy, A. Chemtob, *Microporous Mesoporous Mater.* **2018**, *257*, 42.
[18] a) Y. Gao, J. Lalevée, A. Simon-Masseron, *Adv. Mater. Technol.* **2023**, *8*, 2300377; b) R. S. Ambekar, B. Kushwaha, P. Sharma, F. Bosia, M. Fraldi, N. M. Pugno, C. S. Tiwary, *Mater. Today* **2021**, *48*, 72; c) R. S. Ambekar, E. F. Oliveira, B. Kushwaha, V. Pal, L. D. Machado, S. M. Sajadi, R. H. Baughman, P. M. Ajayan, A. K. Roy, D. S. Galvao, C. S. Tiwary, *Addit. Manuf.* **2021**, *37*, 101628; d) K. P. Barbian, L. T. Hirschwald, J. Linkhorst, M. Neidlin, U. Steinseifer, M. Wessling, B. Wiegmann, S. V. Jansen, *J. Membr. Sci.* **2024**, *690*, 122160.
[19] S. C. Ligon, R. Liska, J. Stampfl, M. Gurr, R. Mülhaupt, *Chem. Rev.* **2017**, *117*, 10212.
[20] F. Rezaei, D. O. Carlsson, J. Hedin Dahlstrom, J. Lindh, S. Johansson, *Sci. Rep.* **2023**, *13*, 22044.
[21] S. A. Rasaki, D. Xiong, S. Xiong, F. Su, M. Idrees, Z. Chen, *J. Adv. Ceram.* **2021**, *10*, 442.
[22] Z. Chen, Z. Li, J. Li, C. Liu, C. Lao, Y. Fu, C. Liu, Y. Li, P. Wang, Y. He, *J. Eur. Ceram. Soc.* **2019**, *39*, 661.
[23] M. Layani, X. Wang, S. Magdassi, *Adv. Mater.* **2018**, *30*, 1706344.
[24] a) H. Seitz, W. Rieder, S. Irsen, B. Leukers, C. Tille, *J. Biomed. Mater. Res., Part B* **2005**, *74*, 782; b) Y. Wen, S. Xun, M. Haoye, S. Baichuan, C. Peng, L. Xuejian, Z. Kaihong, Y. Xuan, P. Jiang, L. Shibi, *Biomater. Sci.* **2017**, *5*, 1690.
[25] A. Butscher, M. Bohner, S. Hofmann, L. Gauckler, R. Müller, *Acta Biomater.* **2011**, *7*, 907.
[26] T. Konegger, L. F. Williams, R. K. Bordia, *J. Am. Ceram. Soc.* **2015**, *98*, 3047.
[27] a) R. P. Chaudhary, C. Parameswaran, M. Idrees, A. S. Rasaki, C. Liu, Z. Chen, P. Colombo, *Prog. Mater. Sci.* **2022**, *128*, 100969; b) M. Das, A. Jana, A. Dixit, R. Mishra, S. Maity, K. R, S. S. Basha, P. Maiti, S. K. Panda, A. Arora, P. S. Owuor, C. S. Tiwary, *Ceram. Int.* **2023**, *49*, 29274; c) M. Das, K. R, S. P. R, A. Jana, A. Dixit, S. K. Panda, D. Roy, C. S. Tiwary, *ACS Sustainable Chem. Eng.* **2023**, *11*, 14308.
[28] L. Li, P. Zhang, Z. Zhang, Q. Lin, Y. Wu, A. Cheng, Y. Lin, C. M. Thompson, R. A. Smaldone, C. Ke, *Angew. Chem.* **2018**, *130*, 5199.
[29] F. Putz, S. Scherer, M. Ober, R. Morak, O. Paris, N. Hüsing, *Adv. Mater. Technol.* **2018**, *3*, 1800060.
[30] a) H. Quan, T. Zhang, H. Xu, S. Luo, J. Nie, X. Zhu, *Bioact. Mater.* **2020**, *5*, 110; b) G. Konstantinou, E. Kakkava, L. Hagelüken, P. V. Warriam Sasikumar, J. Wang, M. G. Makowska, G. Blugan, N. Nianias, F. Marone, H. van Swygenhoven, J. Brugger, D. Psaltis, C. Moser, *Addit. Manuf.* **2020**, *35*, 101343; c) A. Selimis, V. Mironov, M. Farsari, *Microelectron. Eng.* **2015**, *132*, 83.
[31] Q. He, T. Tang, Y. Zeng, N. Iradukunda, B. Bethers, X. Li, Y. Yang, *Adv. Funct. Mater.* **2023**, *34*, 2309323.
[32] J. Rouquerol, D. Avnir, C. W. Fairbridge, D. H. Everett, J. M. Haynes, N. Pernicone, J. D. F. Ramsay, K. S. W. Sing, K. K. Unger, *Pure Appl. Chem.* **1994**, *66*, 1739.
[33] F. Kotz, K. Arnold, W. Bauer, D. Schild, N. Keller, K. Sachsenheimer, T. M. Nargang, C. Richter, D. Helmer, B. E. Rapp, *Nature* **2017**, *544*, 337.
[34] I. Cooperstein, E. Shukrun, O. Press, A. Kamyshny, S. Magdassi, *ACS Appl. Mater. Interfaces* **2018**, *10*, 18879.
[35] E. Shukrun, I. Cooperstein, S. Magdassi, *Adv. Sci.* **2018**, *5*, 1800061.
[36] D. G. Moore, L. Barbera, K. Masania, A. R. Studart, *Nat. Mater.* **2020**, *19*, 212.
[37] E. S. Farrell, N. Ganonyan, I. Cooperstein, M. Y. Moshkovitz, Y. Amouyal, D. Avnir, S. Magdassi, *Appl. Mater. Today* **2021**, *24*, 101083.
[38] E. Shukrun Farrell, Y. Schilt, M. Y. Moshkovitz, Y. Levi-Kalisman, U. Raviv, S. Magdassi, *Nano Lett.* **2020**, *20*, 6598.
[39] T. Aubert, J. Y. Huang, K. Ma, T. Hanrath, U. Wiesner, *Nat. Commun.* **2020**, *11*, 4695.
[40] a) M. Thommes, K. Kaneko, A. V. Neimark, J. P. Olivier, F. Rodriguez-Reinoso, J. Rouquerol, K. S. Sing, *Pure Appl. Chem.* **2015**, *87*, 1051; b) K. A. Cychosz, M. Thommes, *Engineering* **2018**, *4*, 559.
[41] A. L. Patterson, *Phys. Rev.* **1939**, *56*, 978.
[42] a) N. Sreedhar, N. Thomas, O. Al-Ketan, R. Rowshan, H. H. Hernandez, R. K. Abu Al-Rub, H. A. Arafat, *J. Membr. Sci.* **2018**, *561*, 89; b) F. M. Baena-Moreno, M. González-Castaño, J. C. Navarro de Miguel, K. U. M. Miah, R. Ossenbrink, J. A. Odriozola, H. Arellano-García, *ACS Sustainable Chem. Eng.* **2021**, *9*, 8198; c) M. A. Alzoubi, O. Al-Ketan, J. Muthusamy, A. P. Sasmito, S. Poncet, *Results Eng.* **2023**, *17*, 100811; d) T. Femmer, A. J. Kuehne, M. Wessling, *Chem. Eng.* **2015**, *273*, 438; e) F. Wiesner, A. Limper, C. Marth, A. Brodersen, M. Wessling, J. Linkhorst, *Adv. Eng. Mater.* **2023**, *25*, 2200986; f) S. M. Sajadi, P. S. Owuor, S. Schara, C. F. Woellner, V. Rodrigues, R. Vajtai, J. Lou, D. S. Galvão, C. S. Tiwary, P. M. Ajayan, *Adv. Mater.* **2018**, *30*, 1704820.
[43] A. Calvo, P. C. Angelomé, V. M. Sánchez, D. A. Scherlis, F. J. Williams, G. J. A. A. Soler-Illia, *Chem. Mater.* **2008**, *20*, 4661.
[44] a) N. Herzog, H. Hübner, C. Rüttiger, M. Gallei, A. Andrieu-Brunsen, *Langmuir* **2020**, *36*, 4015; b) J. C. Tom, C. Appel, A. Andrieu-Brunsen, *Soft Matter* **2019**, *15*, 8077; c) L. Zhao, J. J. Mikolei, M. Ceolin, R. Pardehkhorram, L. Czerwenka, A. Andrieu-Brunsen, *Microporous Mesoporous Mater.* **2024**, *366*, 112923.
[45] P. Kunwar, A. Poudel, U. Aryal, R. Xie, Z. J. Geffert, H. Wittmann, T. H. Chiang, M. M. Maye, Z. Li, P. Soman, Meniscus-enabled Projection Stereolithography (MAPS), https://doi.org/10.1101/2023.06.12.544584 (accessed: November 2023).
[46] L. Zhao, D. Spiehl, M. C. Kohnen, M. Ceolin, J. J. Mikolei, R. Pardehkhorram, A. Andrieu-Brunsen, *Small* **2024**, 2311121.